Supplementary Information

Co-doped RuO_2 nanoparticles with enhanced catalytic activity and stability for oxygen evolution reaction

Wei Zhang[1], Jiabing Luo[1], Han Tang[1], Shutao Wang[2], Wenle Li[1], Jun Zhang[1], Yan Zhou[1,*]

1. School of Materials Science and Engineering, China University of Petroleum (East China), Qingdao 266580, CHINA (yanzhou@upc.edu.cn)
2. College of Chemistry and Chemical Engineering, China University of Petroleum (East China), Qingdao 266580, CHINA

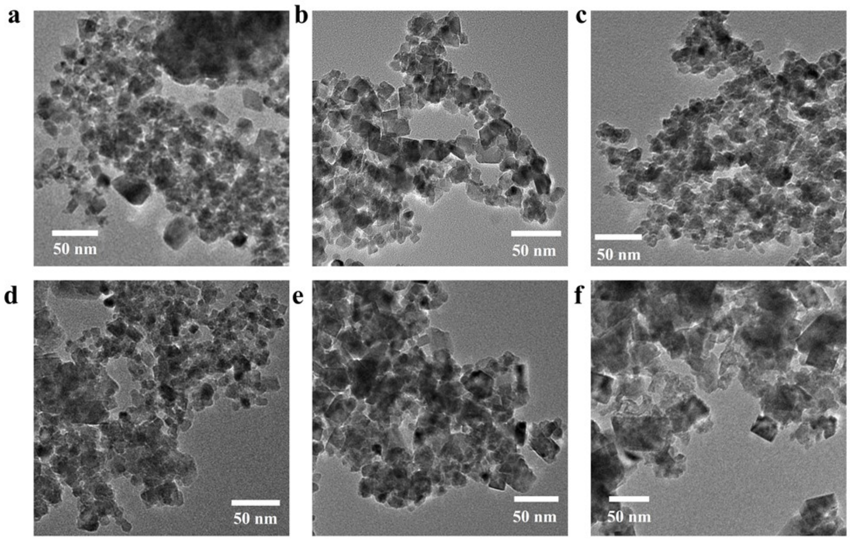

Fig. S1. TEM images of (a) homemade RuO_2, (b) $Ru_{0.98}Co_{0.02}O_y$, (c) $Ru_{0.94}Co_{0.06}O_y$, (d) $Ru_{0.92}Co_{0.08}O_y$, (e) $Ru_{0.86}Co_{0.14}O_y$, (f) $Ru_{0.71}Co_{0.29}O_y$.

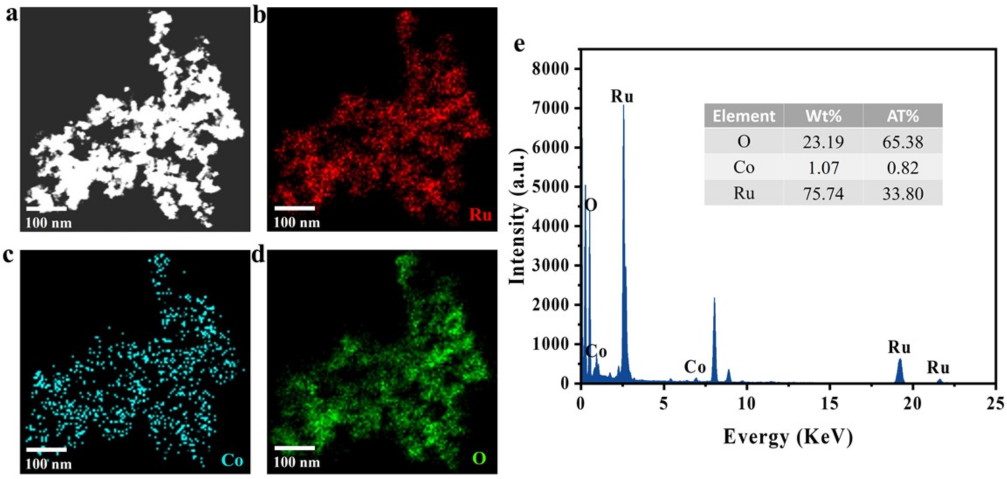

Fig. S2. (a) HAADF-STEM image, EDS elemental mapping of $Ru_{0.98}Co_{0.02}O_y$ for Ru(b), Co(c), O(d), and (e) corresponding EDS spectrum.

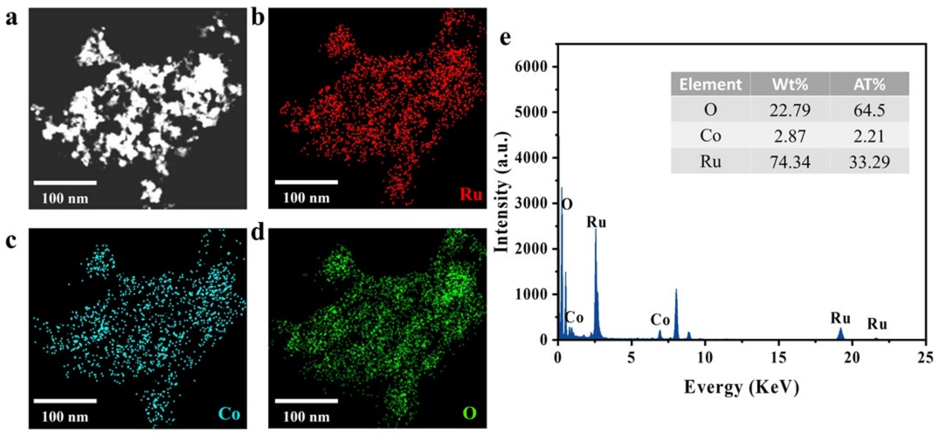

Fig. S3. (a) HAADF-STEM image, EDS elemental mapping of $Ru_{0.94}Co_{0.06}O_y$ for Ru(b), Co(c), O(d), and (e) corresponding EDS spectrum.

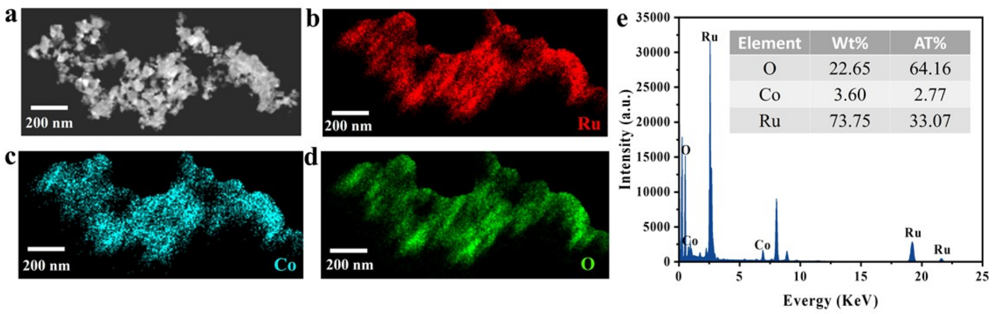

Fig. S4. (a) HAADF-STEM image, EDS elemental mapping of $Ru_{0.92}Co_{0.08}O_y$ for Ru(b), Co(c), O(d), and (e) corresponding EDS spectrum.

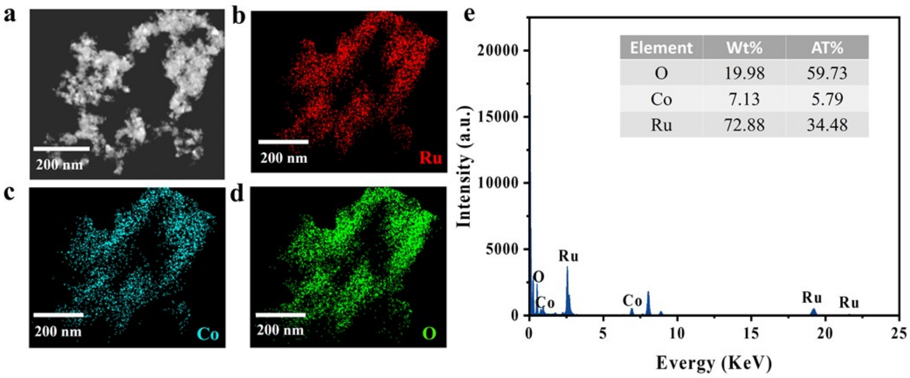

Fig. S5. (a) HAADF-STEM image, EDS elemental mapping of $Ru_{0.86}Co_{0.14}O_y$ for Ru(b), Co(c), O(d), and (e) corresponding EDS spectrum.

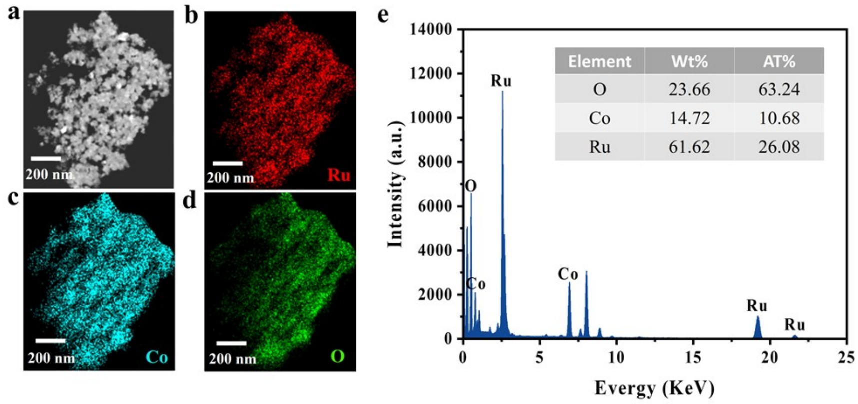

Fig. S6. (a) HAADF-STEM image, EDS elemental mapping of $Ru_{0.71}Co_{0.29}O_y$ for Ru(b), Co(c), O(d), and (e) corresponding EDS spectrum.

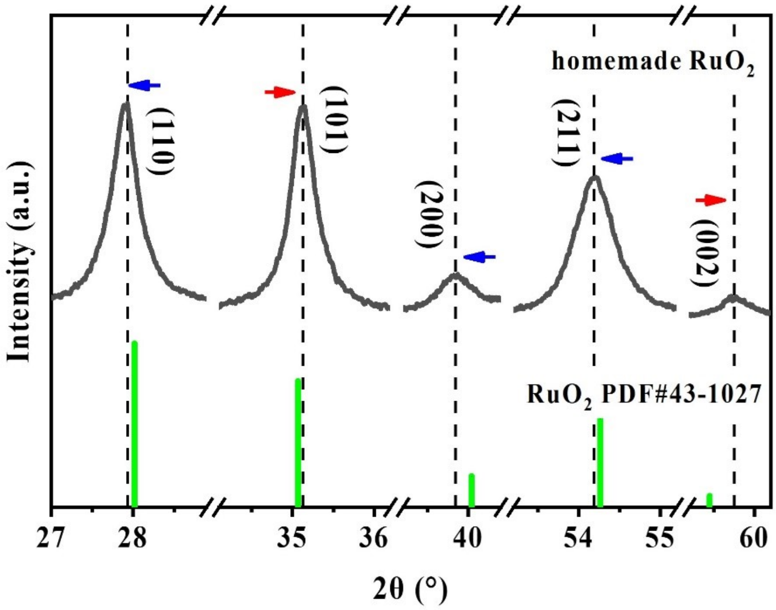

Fig. S7. Datails of XRD pattern of homemade RuO_2 for the diffraction peak of (110), (101), (200), (211), (002) crystal planes.

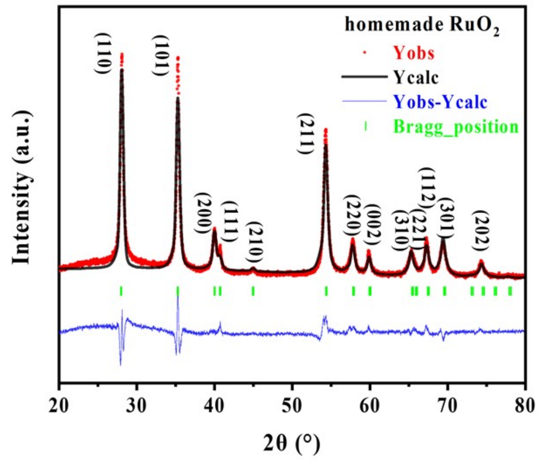

Fig. S8. Rietveld refinement of XRD patterns for homemade RuO_2.

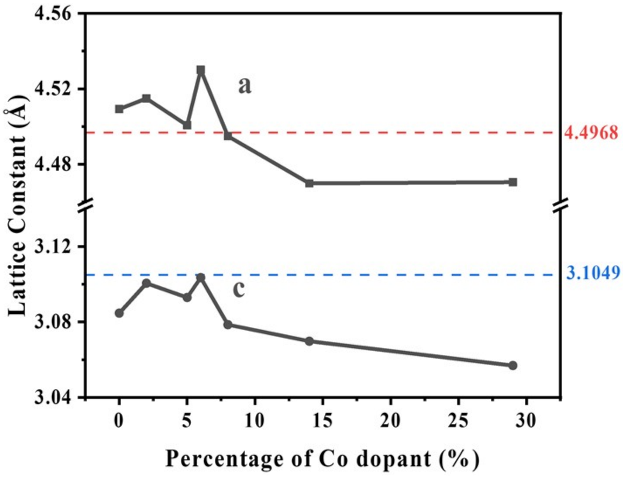

Fig. S9. Lattice constant of $Ru_{1-x}Co_xO_y$ from XRD refinement by Rietveld techniques, with the red and blue dashed lines correspond to the lattice constants a and c of the standard RuO_2 crystal respectively.

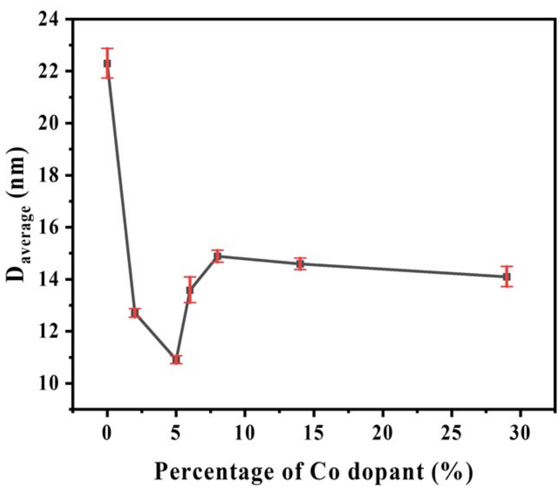

Fig. S10. The average grain size of $Ru_{1-x}Co_xO_y$ calculated from Scherrer equation. The error bars represents the systematic error of calculation based on Scherrer equation.

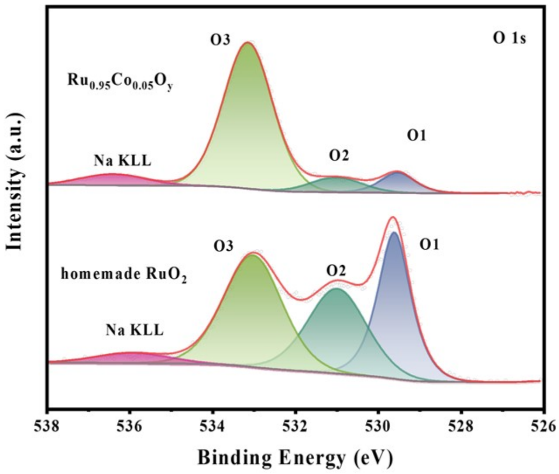

Fig. S11. High-resolution XPS spectra of O 1s orbitals of $Ru_{0.95}Co_{0.05}O_y$.

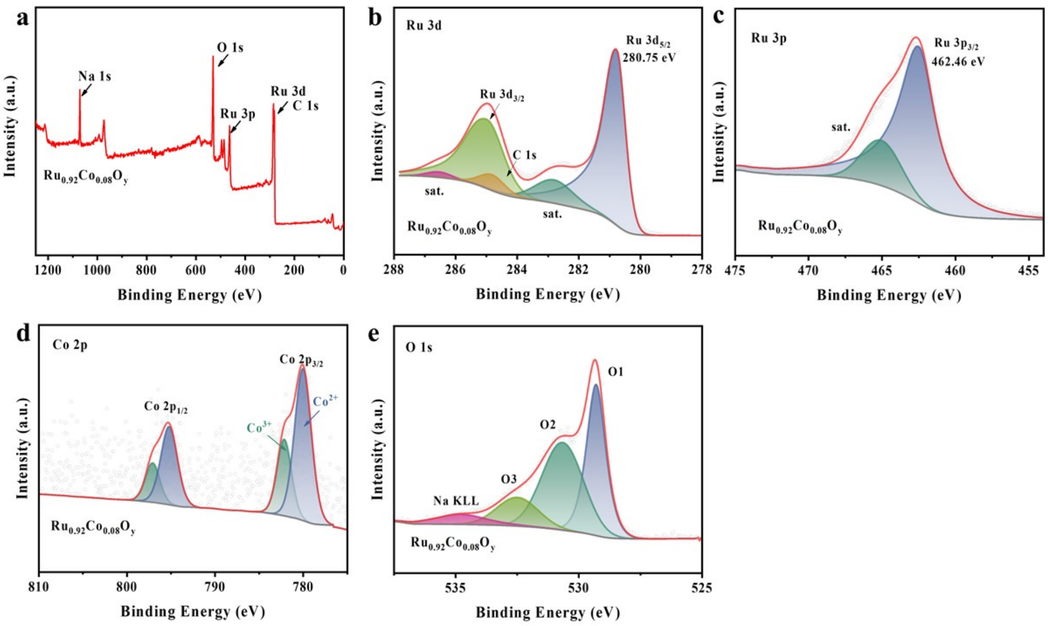

Fig. S12. (a) XPS full spectra of $Ru_{0.92}Co_{0.08}O_y$ and high-resolution XPS spectra of (b) Ru 3d, (c) Ru 3p, (d) Co 2p, (e) O 1s orbitals of $Ru_{0.92}Co_{0.08}O_y$.

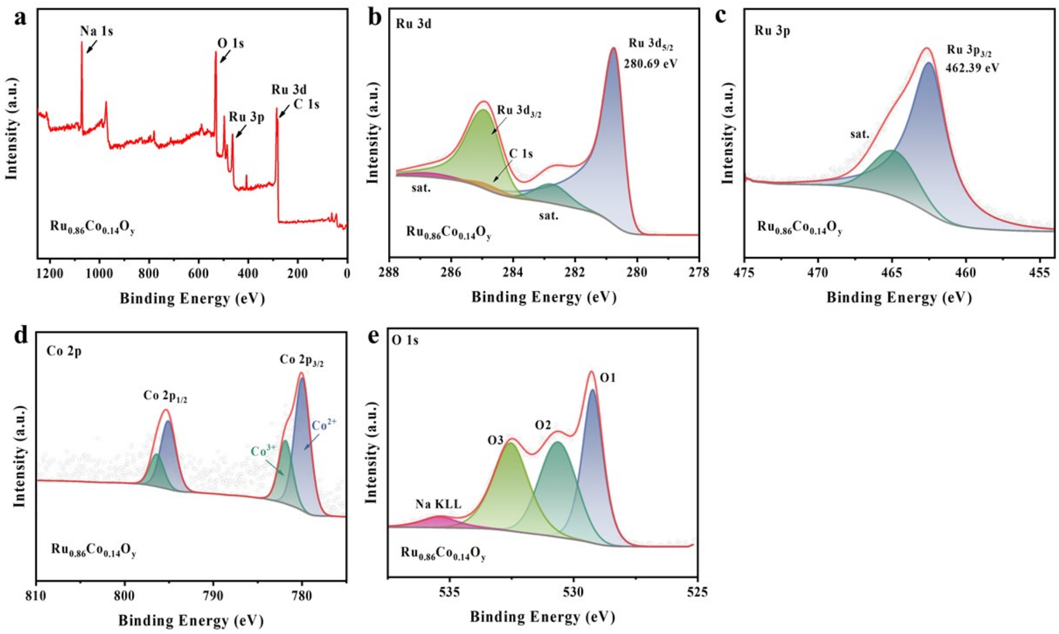

Fig. S13. (a) XPS full spectra of $Ru_{0.86}Co_{0.14}O_y$ and high-resolution XPS spectra of (b) Ru 3d, (c) Ru 3p, (d) Co 2p, (e) O 1s orbitals of $Ru_{0.86}Co_{0.14}O_y$.

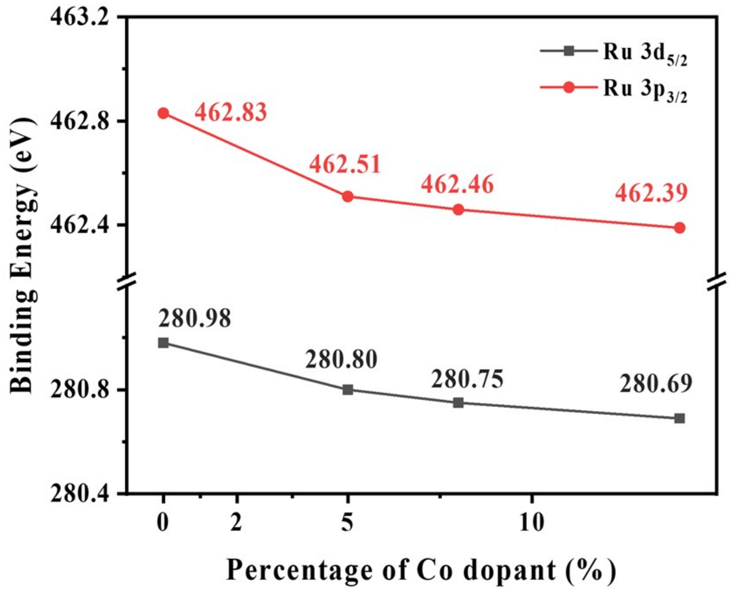

Fig. S14. The position of the Ru XPS peaks in relation to the percentage of Co.

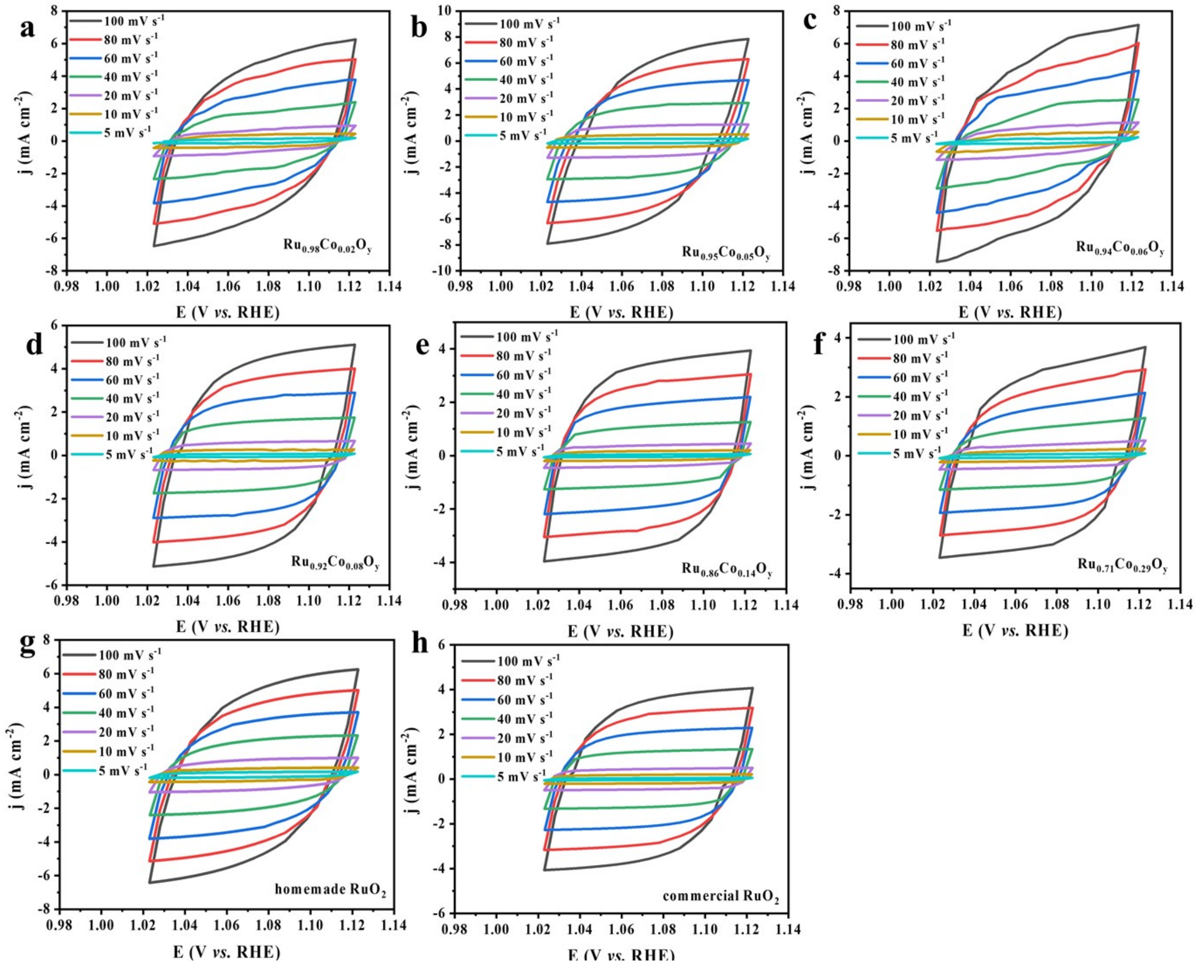

Fig. S15. CV curves in a non-Faradic region (1.024~1.124 V vs. RHE) at different scan rates of (a) $Ru_{0.98}Co_{0.02}O_y$, (b) $Ru_{0.95}Co_{0.05}O_y$, (c) $Ru_{0.94}Co_{0.06}O_y$, (d) $Ru_{0.92}Co_{0.08}O_y$, (e) $Ru_{0.86}Co_{0.14}O_y$, (f) $Ru_{0.71}Co_{0.29}O_y$. (g) homemade RuO_2 and (h) commercial RuO_2.

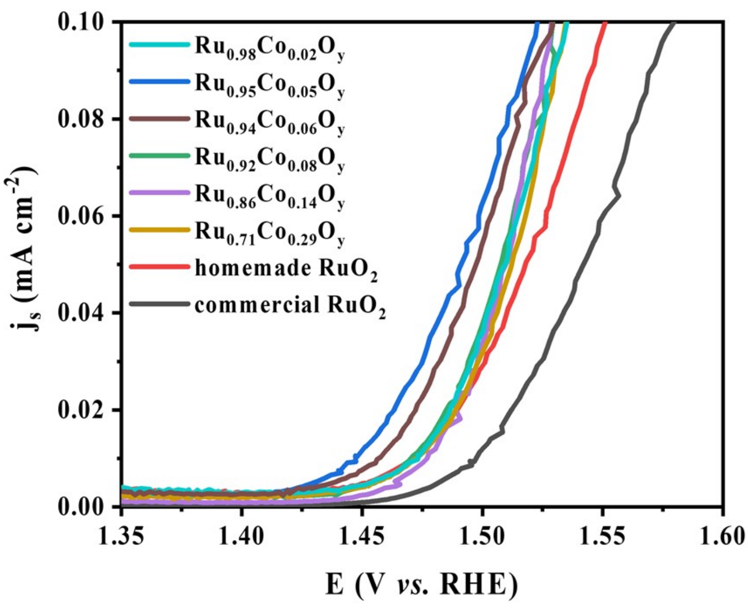

Fig. S16. Normalized LSV curves to electrochemically active surface area.

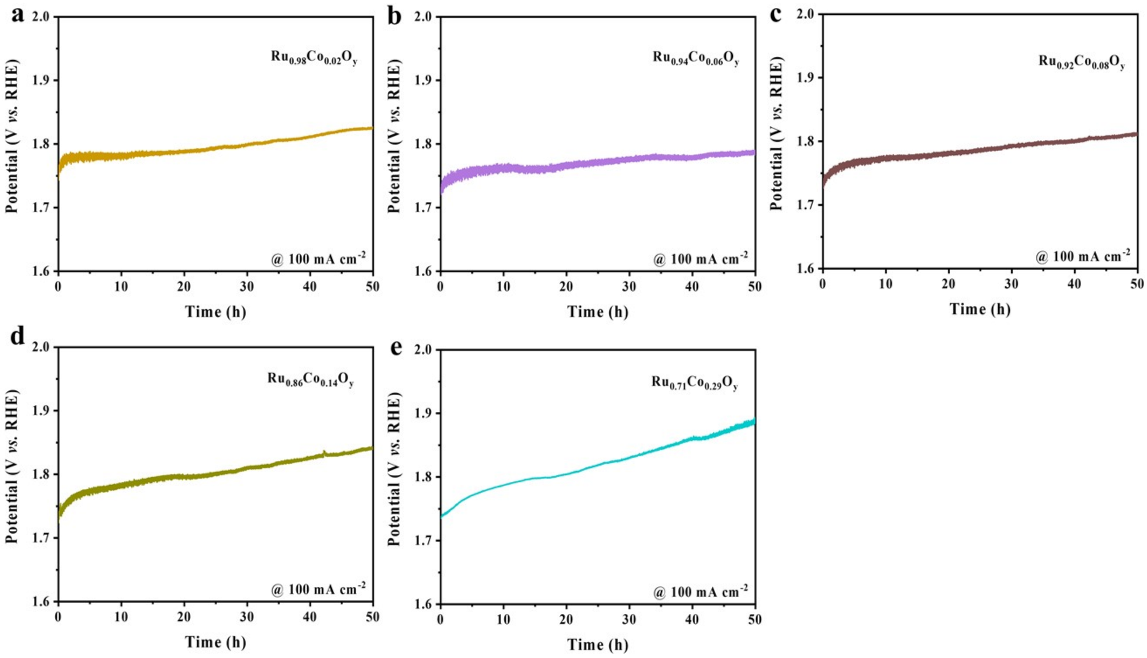

Fig. S17. Chronopotentiometric response (V-t) curves of (a) $Ru_{0.98}Co_{0.02}O_y$, (b) $Ru_{0.94}Co_{0.06}O_y$, (c) $Ru_{0.92}Co_{0.08}O_y$, (d) $Ru_{0.86}Co_{0.14}O_y$, (e) $Ru_{0.71}Co_{0.29}O_y$ at current densities of 100 mA cm^{-2}.

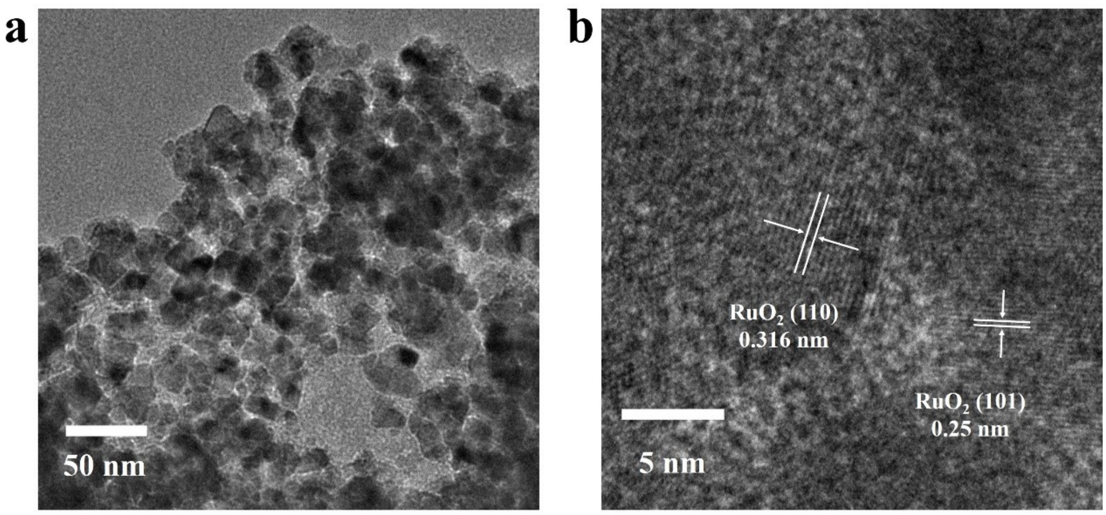

Fig. S18. (a) TEM images and (b) HRTEM images of $Ru_{0.95}Co_{0.05}O_y$ after continuous operation for 50 h at current density of 100 mA cm^{-2}.

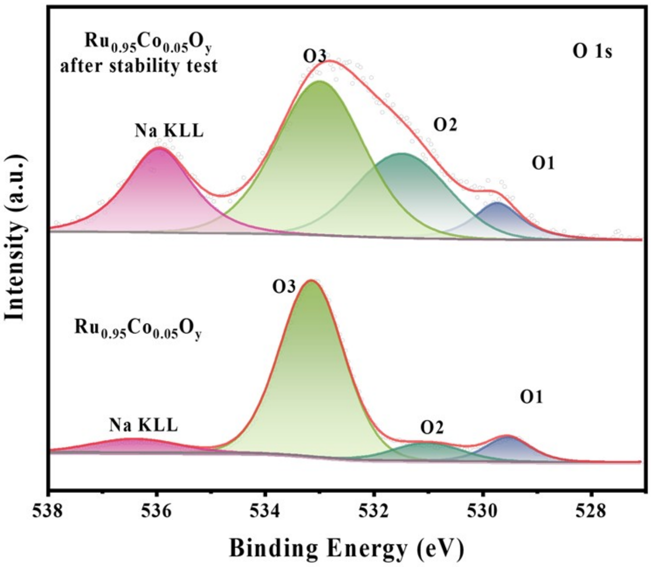

Fig. S19. High-resolution XPS spectra of Co 2p orbitals of $Ru_{0.95}Co_{0.05}O_y$ after stability test.

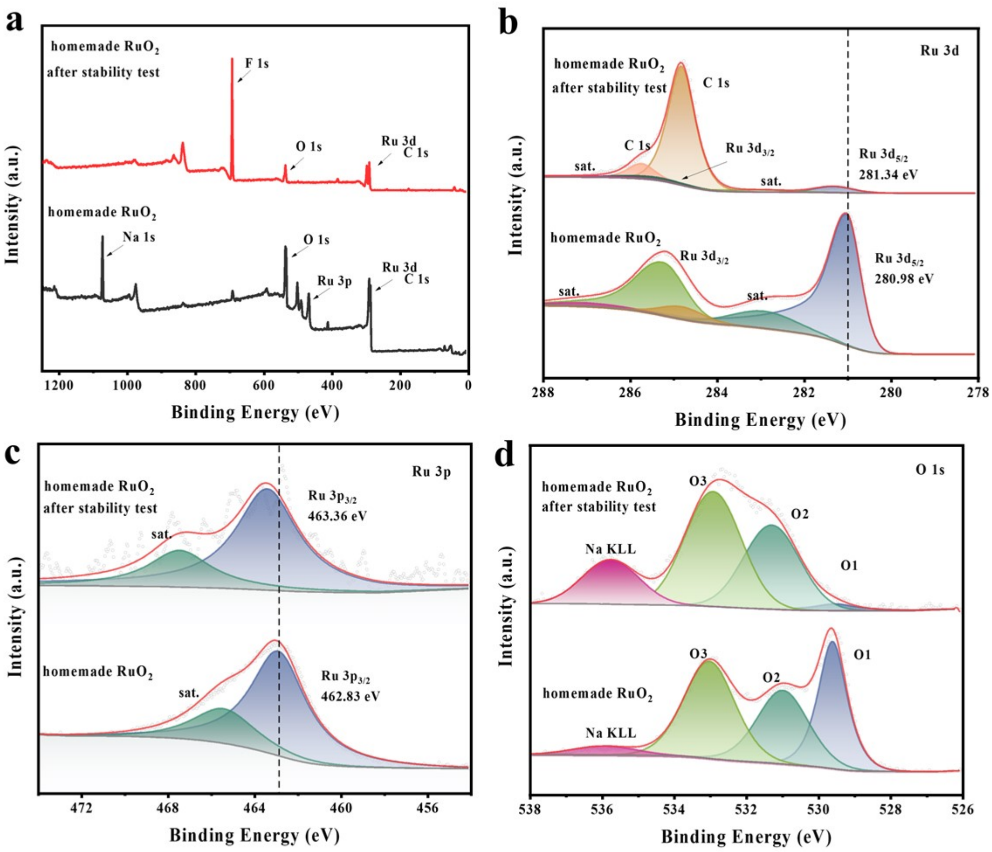

Fig. S20. (a) XPS full spectra and high-resolution XPS spectra of (b) Ru 3d, (c) Ru 3p and (d) O 1s orbitals of homemade RuO_2 after stability test.

Table S1. The content of Ru, Co, O in $Ru_{1-x}Co_xO_y$ etermined by EDS elemental mapping.

	At%			Percentage of Co in metal atoms(%)
	O	Ru	Co	
$Ru_{0.98}Co_{0.02}O_y$	65.38	33.8	0.82	2.37
$Ru_{0.95}Co_{0.05}O_y$	60.98	36.99	2.03	5.20
$Ru_{0.94}Co_{0.06}O_y$	64.5	33.29	2.21	6.23
$Ru_{0.92}Co_{0.08}O_y$	64.16	33.07	2.77	7.73
$Ru_{0.86}Co_{0.14}O_y$	59.73	34.48	5.79	14.38
$Ru_{0.71}Co_{0.29}O_y$	63.24	26.08	10.68	29.05

Table S2. Lattice constant of $Ru_{1-x}Co_xO_y$ from XRD refinement by Rietveld techniques

Percentage of Co dopant (%)	Lattice Constant (Å)	
	a	c
0	4.50923 ± 0.00076	3.08466 ± 0.0006
2	4.51484 ± 0.00299	3.10048 ± 0.00199
5	4.50061 ± 0.00284	3.09294 ± 0.00186
6	4.53003 ± 0.00267	3.10346 ± 0.00183
8	4.49488 ± 0.00156	3.07856 ± 0.00099
14	4.46988 ± 0.00173	3.06978 ± 0.00108
29	4.47050 ± 0.00289	3.00289 ± 0.00185

Table S3. The content of Ru, Co, O in $Ru_{0.95}Co_{0.05}O_y$ after the *V-t* test determined by EDS elemental mapping.

	Wt%	At%	Percentage in metal atoms(%)
O	23.18	65.12	--
Co	2.3	1.75	5.02
Ru	74.52	33.13	94.98

Table S4. Comparison of OER catalytic performance with previously reported noble-metal-based electrocatalysts in alkaline electrolyte.

Catalyst	Overpotential [a] (mV)	Tafel (mV dec^{-1})	Stability [b] (h)	Reference
$Ru_{0.95}Co_{0.05}O_y$	217 (@10 mA cm^{-2}) 290 (@100 mA cm^{-2})	50.83	50 (@100 mA cm^{-2})	This work
Homemade RuO_2	281	61.5	50 (@100 mA cm^{-2})	
Ru-$NiCo_2O_4$ NSs	230	79	42	1
RuCu NSs/C	234	-	12	2
a/cRuO_2	235	43.6	24	3
Ru_1Co_2 NPs	240	54.4	8	4
$RuIrO_x$	250	50	-	5
RuO_2/NiO/NF	250	50.5	24	6
Li-$IrSe_2$	270	-	10	7
$Ru_{0.7}Co_{0.3}$ aerogel	272	41.6	12.5 (@100 mA cm^{-2})	8
Ir@Co NSs	273	99	10	9
IrO_2@SL-NiFe LDHs	274	59	35	10
Ru-MoS_2-Mo_2C/TiN	280	202	50 (@20 mA cm^{-2})	11
$NiCo_{1.7}Ru_{0.3}O_4$	280	78	15	12
RuCo@NC	280	91	24	13
a-$RuTe_2$ PNRs	285	62	-	14
RuO_2@NPC	290	64	8.33	15
Ir-NR/C	296	60.3	-	16
RuO_2/Co_3O_4 NBs	302	75.77	-	17
CoRu–MoS_2	308	50	16	18
Ru@RuO_2 core-shell nanorods	320	86	25	19
Ru_2Ni_2 SNs/C	357	75	-	20
CoNiRu-NT	255 (@20 mA cm^{-2}) 335 (@100 mA cm^{-2})	67	48 (@100 mA cm^{-2})	21

a: Overpotential at the current density of 10 mA cm^{-2} unless specifically marked.

b: Stability tests at the current density of 10 mA cm^{-2} unless specifically marked.

Table S5. Comparison of noble metal losses during OER durability test.

Catalyst	Stability operation time [a] (h)	Noble metal loss (%)	Reference
$RuCoO_y$-2	50 (@100 mA cm^{-2})	0.058	This work
Homemade RuO_2	50 (@100 mA cm^{-2})	0.12	
a/cRuO_2	24	2.04	[3]
Li-$IrSe_2$	10 (@20 mA cm^{-2})	0.38	[7]
SrTi(Ir)O_3	10	0.44	[22]
$RuNi_x$@G-T	24	1.5	[23]
$CaCu_3Ru_4O_{12}$	24	2.7	[24]
Ru-N-C	30	5	[25]

a: Stability tests at the current density of 10 mA cm^{-2} unless specifically marked.

Reference

1. R. Yang, X. Shi, Y. Wang, J. Jin, H. Liu, J. Yin, Y.-Q. Zhao and P. Xi, *Chinese Chemical Letters*, 2022, **33**, 4930-4935.
2. Q. Yao, B. Huang, N. Zhang, M. Sun, Q. Shao and X. Huang, *Angewandte Chemie International Edition*, 2019, **58**, 13983-13988.
3. L. Zhang, H. Jang, H. Liu, M. G. Kim, D. Yang, S. Liu, X. Liu and J. Cho, *Angewandte Chemie International Edition*, 2021, **60**, 18821-18829.
4. Y. Bao, J. Dai, J. Zhao, Y. Wu, C. Li, L. Ji, X. Zhang and F. Yang, *ACS Applied Energy Materials*, 2020, **3**, 1869-1874.
5. Z. Zhuang, Y. Wang, C.-Q. Xu, S. Liu, C. Chen, Q. Peng, Z. Zhuang, H. Xiao, Y. Pan, S. Lu, R. Yu, W.-C. Cheong, X. Cao, K. Wu, K. Sun, Y. Wang, D. Wang, J. Li and Y. Li, *Nature Communications*, 2019, **10**.
6. J. Liu, Y. Zheng, Y. Jiao, Z. Wang, Z. Lu, A. Vasileff and S. Z. Qiao, *Small*, 2018, **14**.
7. T. Zheng, C. Shang, Z. He, X. Wang, C. Cao, H. Li, R. Si, B. Pan, S. Zhou and J. Zeng, *Angewandte Chemie International Edition*, 2019, **58**, 14764-14769.
8. Z. Lin, S. Liu, Y. Liu, Z. Liu, S. Zhang, X. Zhang, Y. Tian and Z. Tang, *Journal of Power Sources*, 2021, **514**.
9. D. D. Babu, Y. Huang, G. Anandhababu, X. Wang, R. Si, M. Wu, Q. Li, Y. Wang and J. Yao, *Journal of Materials Chemistry A*, 2019, **7**, 8376-8383.
10. D. Li, T. Li, G. Hao, W. Guo, S. Chen, G. Liu, J. Li and Q. Zhao, *Chemical Engineering Journal*, 2020, **399**.
11. V. H. Hoa, D. T. Tran, S. Prabhakaran, D. H. Kim, N. Hameed, H. Wang, N. H. Kim and J. H. Lee, *Nano Energy*, 2021, **88**.
12. C. Peng, H. Liu, J. Chen, Y. Zhang, L. Zhu, Q. Wu, W. Zou, J. Wang, Z. Fu and Y. Lu, *Applied Surface Science*, 2021, **544**.

13. B. Sarkar, D. Das and K. K. Nanda, *Green Chemistry*, 2020, **22**, 7884-7895.
14. J. Wang, L. Han, B. Huang, Q. Shao, H. L. Xin and X. Huang, *Nature Communications*, 2019, **10**.
15. N. Wang, S. Ning, X. Yu, D. Chen, Z. Li, J. Xu, H. Meng, D. Zhao, L. Li, Q. Liu, B. Lu and S. Chen, *Applied Catalysis B: Environmental*, 2022, **302**.
16. F. Luo, L. Guo, Y. Xie, J. Xu, K. Qu and Z. Yang, *Applied Catalysis B: Environmental*, 2020, **279**.
17. B.-Y. Guo, X.-Y. Zhang, X. Ma, T.-S. Chen, Y. Chen, M.-L. Wen, J.-F. Qin, J. Nan, Y.-M. Chai and B. Dong, *International Journal of Hydrogen Energy*, 2020, **45**, 9575-9582.
18. I. S. Kwon, T. T. Debela, I. H. Kwak, Y. C. Park, J. Seo, J. Y. Shim, S. J. Yoo, J. G. Kim, J. Park and H. S. Kang, *Small*, 2020, **16**.
19. R. Jiang, D. T. Tran, J. Li and D. Chu, *Energy & Environmental Materials*, 2019, **2**, 201-208.
20. J. Ding, Q. Shao, Y. Feng and X. Huang, *Nano Energy*, 2018, **47**, 1-7.
21. Y. Wang, S. Wang, Z. L. Ma, L. T. Yan, X. B. Zhao, Y. Y. Xue, J. M. Huo, X. Yuan, S. N. Li and Q. G. Zhai, *Advanced Materials*, 2022, **34**.
22. H. Chen, L. Shi, X. Liang, L. Wang, T. Asefa and X. Zou, *Angewandte Chemie International Edition*, 2020, **59**, 19654-19658.
23. X. Cui, P. Ren, C. Ma, J. Zhao, R. Chen, S. Chen, N. P. Rajan, H. Li, L. Yu, Z. Tian and D. Deng, *Advanced Materials*, 2020, **32**.
24. X. Miao, L. Zhang, L. Wu, Z. Hu, L. Shi and S. Zhou, *Nature Communications*, 2019, **10**.
25. L. Cao, Q. Luo, J. Chen, L. Wang, Y. Lin, H. Wang, X. Liu, X. Shen, W. Zhang, W. Liu, Z. Qi, Z. Jiang, J. Yang and T. Yao, *Nature Communications*, 2019, **10**.